공학석사 학위논문

Evaluation of Deformation Characteristics of Soil Ground against Ground Cave-in Caused by Damaged Pipe using Generalized Interpolation Material Point Method (GIMP)

Generalized Interpolation Material Point Method (GIMP)를 이용한 하수관 손상에 의한 지반 함몰 발생 시 지반의 변형 특성 평가

2018년 1월

서울대학교 대학원

건설환경 공학부

이 민 호

Evaluation of Deformation Characteristics of Soil Ground against Ground Cave-in Caused by Damaged Pipe using Generalized Interpolation Material Point Method (GIMP)

Generalized Interpolation Material Point Method (GIMP)를 이용한 하수관 손상에 의한 지반 함몰 발생 시 지반의 변형 특성 평가

지도 교수 정 충 기

이 논문을 공학석사 학위논문으로 제출함

2018년 1월

서울대학교 대학원

건설환경공학부

이 민 호

이민호 석사 학위논문을 인준함

2018년 1월

위 원 장 박 준 범 (인)

부위원장 정 충 기 (인)

위 원 우 상 인 (인)

Abstract

Evaluation of Deformation Characteristics of Soil Ground against Ground Cave-in Caused by Damaged Pipe using Generalized Interpolation Material Point Method (GIMP)

Lee, Min Ho

Department of Civil and Environmental Engineering

The Graduate School

Seoul National University

As the number of ground cave-in occurred in Seoul and the social costs associated with the ground cave-ins are increasing, the ground cave-ins are in the spotlight as one of the major ground hazards which can be occurred in urban area. Most of the ground cave-ins occurred in urban area is mainly due to damaged sewer pipe. If there is a crack on a sewer pipe, water flows out of the crack when the damaged sewer pipe is filled with water. After that, water flows into the crack with soil around the sewer pipe. As this process repeating, a cavity is formed near the sewer pipe and this can finally lead to a ground cave-in. When unsaturated ground becomes saturated due to water discharged from a sewer pipe, shear strength of soil decreases and it makes a cavity unstable. In this study, model tests and numerical analysis are performed to investigate the effect of decrease in shear strength of soil induced by the saturation of ground on the formation of a ground cave-in. Unlike model tests which performed by repeating water inflow and outflow, the process of water leakage from the model ground was skipped to investigate the effect of reduction in shear strength of soil and to exclude the effect of seepage force during water leakage. Problems involving large deformation such as a ground cave-in are not properly solved using the finite element method (FEM) as a result of mesh related problems. Generalized

interpolation material point method (GIMP) in which the body is discretized into finite number of material points was used in this study as an alternative to FEM. Though there are differences between the model test and numerical simulation caused by boundary conditions, incomplete saturation, and exclusion of seepage analysis, similar ground deformation characteristics are observed in the model test and numerical simulation

Keywords: Ground cave-in, Shear strength of soil, Degree of saturation, Model test, Generalized interpolation material point method (GIMP)

Student Number: 2015-22929

Contents

List of Tables

List of Figures

Chapter 1 Introduction

1.1 Background

As the number of ground cave-in occurred in Seoul and the social costs associated with the ground cave-ins are increasing, the ground cave-ins are in the spotlight as one of the major ground hazards which can be occurred in urban area. These days, a lot of researchers are putting their effort on preparing measures to prevent ground cave-ins and investigating the mechanism of the phenomenon.

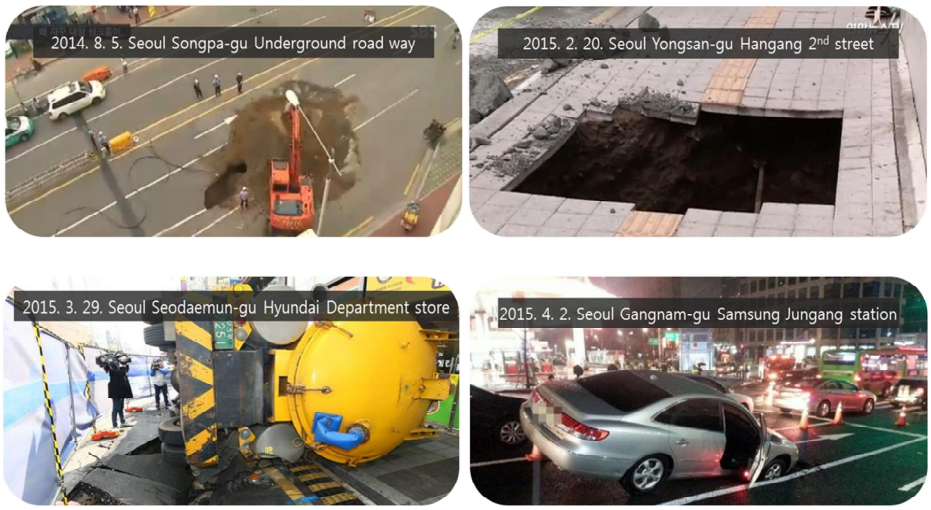

Figure 1.1 Ground cave-ins occurred in Seoul

According to report published by Seoul at 2017, almost 700 ground cave-ins are occurred from 2011 to 2016. Damaged sewer pipes, excavation, and damaged water supply are the three most main causes of ground cave-ins

occurred in Seoul. Among them, 77.4% of ground cave-ins are due to damaged sewer pipe.

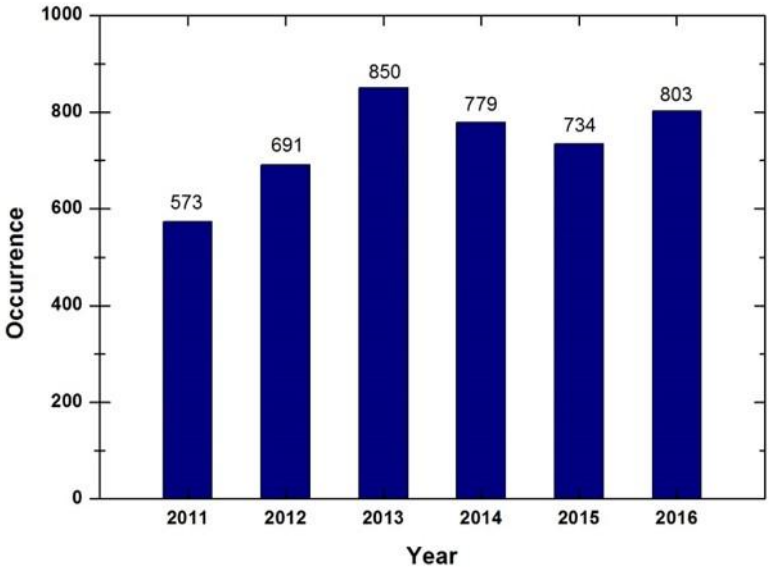

Figure 1.2 Annual occurrence of ground cave-ins occurred in Seoul

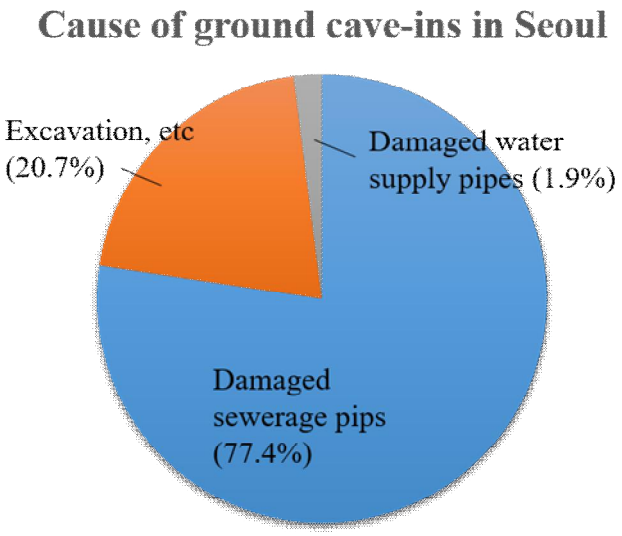

Figure 1.3 Causes of ground cave-ins occurred in Seoul

The process of ground cave-in is illustrated in Figure 1.4

1) Differential settlement of sewer pipe or traffic load acting on the ground causes sewer pipes to crack.
2) Water flows through the crack induces soil near the crack to leak into the sewer pipe and a cavity is formed.
3) Finally, the cavity collapses when it can't support loads acting on it.

In other words, soil loss occurred due to water flow is the main cause of ground cave-in.

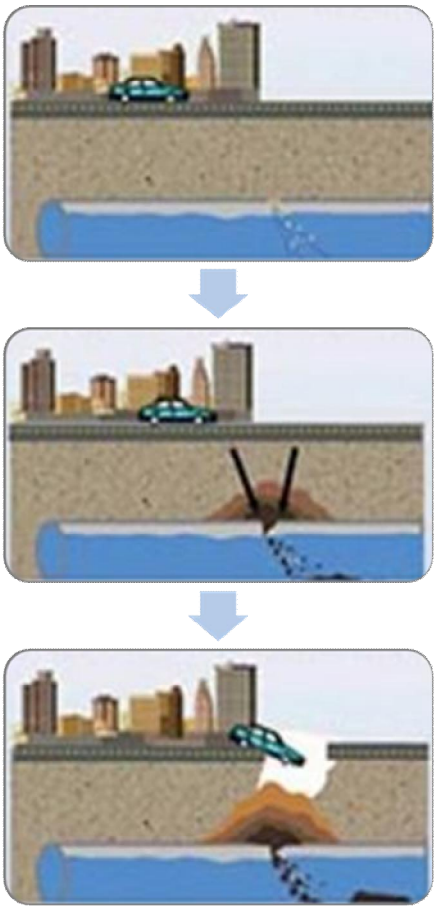

Figure 1.4 Development of ground cave-in induced by damaged sewer

Soil loss is resisted by the shear strength of soil and arching effect as shown in Figure 1.5. When water leakage occurs from the damaged sewer pipe, unsaturated soil ground becomes saturated and it makes shear strength of soil decreases, which reduces resistance against soil loss.

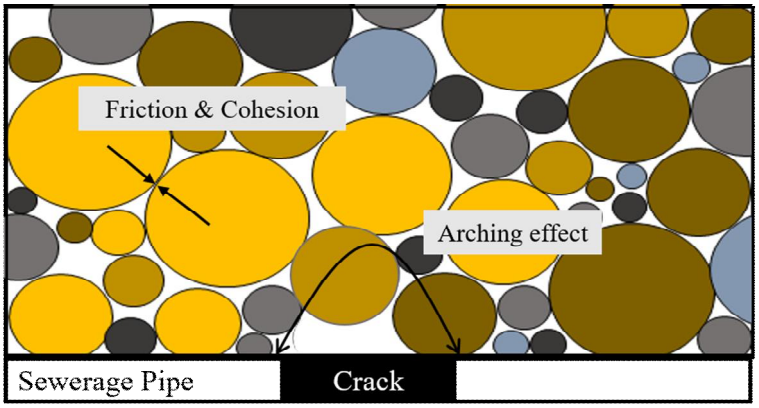

Figure 1.5 Forces acting against soil loss

1.2 Objectives

The main purpose of this study is to evaluate the effect of decrease in shear strength of soil induced by increase in the degree of saturation of soil during formation of ground cave-in caused by damaged sewer pipe. The specific objectives of this study are as follow

1. Investigating the effect of saturation on the development of ground cave-in with model tests.

2. Simulating the model test using generalized interpolation material point method (GIMP) and investigating the applicability of GIMP on ground cave-in

1.3 Thesis Organization

This thesis deals with the assessment of ground movement in the process of developing ground cave-in using model test and numerical analysis.

Chapter 1. Introduction

Introduction includes research background, objectives and thesis organization.

Chapter 2. Literature Review

Literature review for generalized interpolation material point method (GIMP), shear strength of unsaturated soil and model test simulating ground cave-in due to damaged sewer.

Chapter 3. Model Test and Numerical Analysis

Methodologies and results of model test and numerical analysis using GIMP for assessing the effect of saturation on ground cave-ins are described.

Chapter 4. Conclusions

Comparison between results of model test and numerical analysis and summary of this study are described.

Chapter 2 Literature Review

2.1 Generalized Interpolation Material Point Method

For an arbitrary domain Ω, Balance of linear momentum is given by;

$$\sigma_{ij,j} + \rho b_i - \rho a_i = 0 \qquad \text{Equation (1)}$$

Where σ_{ij} is stress, b_i is body force per unit mass, ρ is density, and a_i is acceleration. Equation (1) can be modified by multiplying test function w_i and integrating over the domain Ω of the problem. The modified equation is given by;

$$\int_\Omega w_i \rho a_i \mathrm{d}\Omega = \left[\int_\Gamma w_i t_i \mathrm{d}\Gamma + \int_\Omega w_i \rho b_i \mathrm{d}\Omega \right] - \int_\Omega w_{i,j} \sigma_{ij} \mathrm{d}\Omega \quad \text{Equation (2)}$$

Where t_i (= $\sigma_{ij} n_j$) is surface traction, Γ is the boundary of the domain Ω. In GIMP, the body and space is discretized into finite number of material points and background grid respectively to solve equation (2).

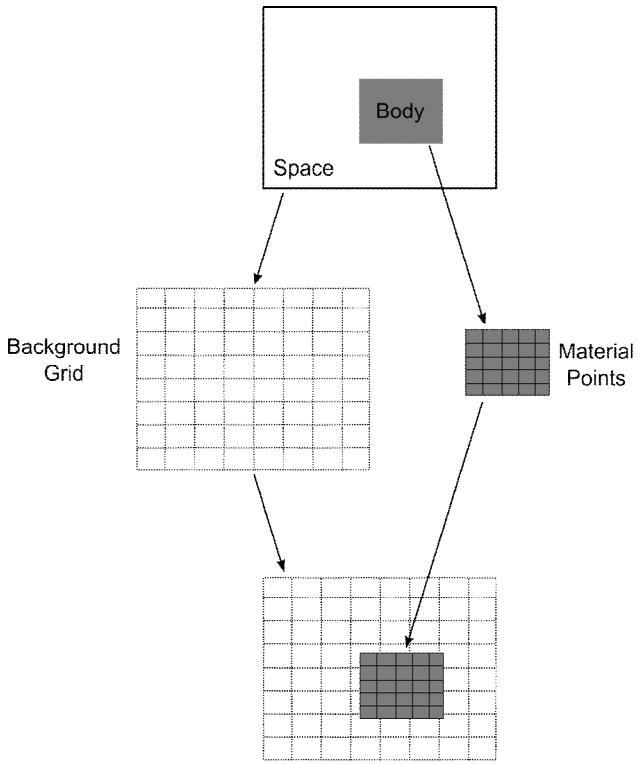

Figure 2.1 GIMP discretization

Material points of GIMP have an area and this area that corresponds to the particle is defined by the particle characteristic function $\chi^{*(P)}$, which has the partition of unity property.

$$\chi^{*(P)}(\mathbf{x}) = \begin{cases} 1 & \mathbf{x} \in \Omega^{*(P)} \\ 0 & \mathbf{x} \notin \Omega^{*(P)} \end{cases} \qquad \text{Equation (3)}$$

Superscript P stands for a material point and $\Omega^{*(P)}$ is the area of material point P. Using particle characteristic function $\chi^{*(P)}$, stress, momentum and density at any point **x** can be computed.

$$\sigma_{ij}(\mathbf{x}) = \sum_P \sigma_{ij}^{(P)} \chi^{*(P)}(\mathbf{x})$$
$$p_i(\mathbf{x}) = \sum_P p_i^{(P)} \chi^{*(P)}(\mathbf{x}) \qquad \text{Equation (4)}$$
$$\rho(\mathbf{x}) = \sum_P \rho^{(P)} \chi^{*(P)}(\mathbf{x})$$

Where $\sigma_{ij}^{(P)}$, $p_i^{(P)}$ and $\rho^{(P)}$ are stress, momentum and density respectively. Using a standard FE shape function $N^{(I)}$ for node I, the value w_i of the test function at any location in the grid occupied by an individual particle can be computed from its values at grid node.

$$w_i(\mathbf{x}) = \sum_I w_i^{(I)} N^{(I)}(\mathbf{x}) \qquad \text{Equation (5)}$$

Where $\sigma_{ij}^{(P)}$, $p_i^{(P)}$ and $\rho^{(P)}$ are stress, momentum and density respectively. Using a standard FE shape function $N^{(I)}$ for node I, the value w_i of the test function at any location in the grid occupied by an individual particle can be computed from its values at grid node. In this study, background grid is consisted of four-node square element, and standard FE shape function $N^{(I)}$ is the same as shape function of finite element method. As the test function w_i is arbitrary, equation (2) becomes equation (5) after GIMP discretization.

$$\dot{p}_i^{(I)} = f_i^{(I)EXT} - f_i^{(I)INT} \qquad \text{Equation (1)}$$

$$f_i^{(I)EXT} = \int_\Gamma t_i N^{(I)} \mathrm{d}\Gamma + \sum_P \left[\frac{1}{V^{*(P)}} \int_{\Omega^{*(P)}} \chi^{*(P)} N^{(I)} \mathrm{d}\Omega \right] m^{(P)} b_i$$
$$= \int_\Gamma t_i N^{(I)} \mathrm{d}\Gamma + \sum_P S^{(IP)} m^{(P)} b_i \qquad \text{Equation (2)}$$

$$f_i^{(I)INT} = \sum_P \left[\frac{1}{V^{*(P)}} \int_{\Omega^{(P)}} \chi^{*(P)} N_{,j}^{(I)} \mathrm{d}\Omega \right] \sigma_{ij}^{(P)} V^{(P)} = \sum_P G_j^{(IP)} \sigma_{ij}^{(P)} V^{(P)}$$

Equation (3)

Where $f_i^{(I)EXT}$ and $f_i^{(I)INT}$ are external force and internal force at node I, respectively. $V^{*(P)}$ is the volume of material point P. $S^{(IP)}$ and $G_j^{(IP)}$ are value of value of a variable at node I from the values of the same variable at the material point P and weighted average of particle characteristic function $\chi^{*(P)}$ respectively. Mass $m^{(I)}$ and momentum $p_i^{(I)}$ at node I are expressed by:

$$m^{(I)} = \sum_P \left[\frac{1}{V^{*(P)}} \int_{\Omega^{*(P)}} \chi^{*(P)} N^{(I)} \mathrm{d}\Omega \right] m^{(P)} = \sum_P S^{(IP)} m^{(P)} \quad \text{Equation (4)}$$

$$p_i^{(I)} = \sum_P \left[\frac{1}{V^{*(P)}} \int_{\Omega^{*(P)}} \chi^{*(P)} N^{(I)} \mathrm{d}\Omega \right] p_i^{(P)} = \sum_P S^{(IP)} p_i^{(P)} \quad \text{Equation (5)}$$

2.2 Shear Strength of Unsaturated Soils

The shear strength of a saturated soil can be defined using the Mohr-Coulomb failure criterion and the effective stress variable (Terzaghi, 1936) as shown in Equation (1). Where τ_{ff} is shear stress on the failure plane at failure, c' is effective cohesion, $(\sigma_f - u_w)_f$ is effective normal stress on the failure plane at failure, ϕ' is effective angle of internal friction.

$$\tau_{ff} = c' + (\sigma_f - u_w)_f \tan\phi' \qquad \text{Equation (1)}$$

In the case of unsaturated soil, the shear strength is influenced by matric suction and shear strength is increased as the matric suction is increased. Fredlund et at. (1978) extended shear strength equation of saturated soil to embrace unsaturated soil and the extended shear strength equation for an unsaturated soil can be expressed using two stress variables, $(\sigma - u_a)$ and $(u_a - u_w)$ as shown in Equation (2). Where $(\sigma_f - u_a)_f$ is net normal stress state on the failure plane at failure, $(u_a - u_w)_f$ is matric suction on the failure plane at failure, ϕ^b is angle indicating the rate of increase in shear strength with respect to a change in matric suction. The shear strength change with respect to matric suction is defined by the angle ϕ^b.

$$\tau_{ff} = c' + (\sigma_f - u_a)_f \tan\phi' + (u_a - u_w)_f \tan\phi^b \qquad \text{Equation (2)}$$

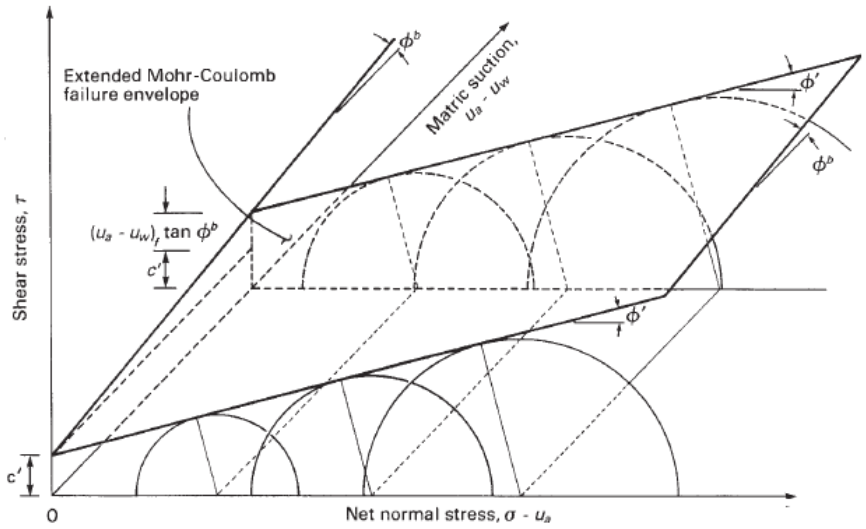

Figure 2.2 Extended Mohr-Coulomb failure envelope for unsaturated soils.

By including matric suction component in the cohesion component of shear strength, Equation (2) can be written as Equation (3). Where c is apparent cohesion, $c = c' + (u_a - u_w)_f \tan\phi^b$.

$$\tau_{ff} = c + (\sigma_f - u_a)_f \tan\phi' \qquad \text{Equation (3)}$$

As soil becomes saturated, matric suction goes to zero and apparent cohesion decreases. Consequently, the shear strength of soil decreases.

2.2 Previous Model Tests for Ground Cave-in

2.2.1 Model Test Conducted in Japan

Kuwano et al. (2010) conducted model test simulating leakage of soil through a crack on a damaged sewer pipe to investigate the mechanism and factors which influence formation of ground cave-in. The Test equipment consists of two part, soil chamber and external water supply tank. The test is conducted by repeating water flows in and out into the soil chamber from external water supply tank to simulate the procedure of formation of ground cave-in caused by damaged sewer pipe.

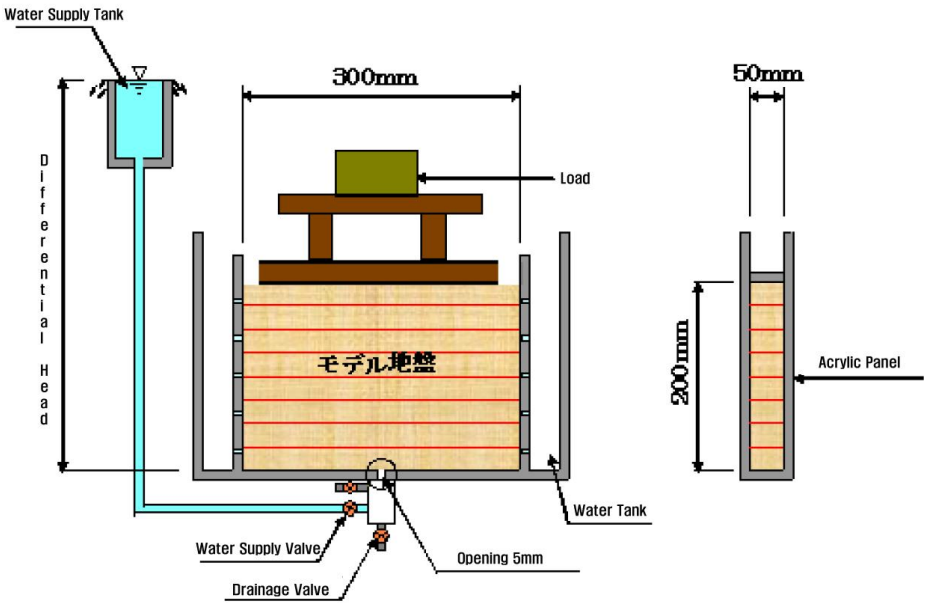

Figure 2.3 Test Equipment used in the model test

According to the results, model ground becomes unstable as matric suction decreases when water flows into the model ground. The soil loss

through the opening occurs as water flow out of the model ground which forms a cavity and loosening in the ground. Increase in degree of saturation of soil causes shear strength of soil decreased which is the key factor that lead to soil loss and ground cave-in.

Chapter 3 Model Test and Numerical Analysis

3.1 Direct Shear Test for Saturated and Unsaturated Soil

Strength parameters used in the numerical analysis is taken from direct shear test. Soil used in direct shear test is soil used in model test. In saturated and unsaturated condition, direct shear test was conducted for the specimen compacted 92% and 84% of maximum dry unit weight of soil. Each specimen was compacted at the optimum moist content obtained from standard compaction test. To make saturated soil, specimen was inundated and kept weighing the specimen. The specimen was considered to be saturated when weight of the soil sample was constant. (Kim and Kim, 2010) It took 3 hours to make soil sample saturated. The tests were conducted at normal stress of 40, 80, 160 kPa and sheared the sample until horizontal displacement reached to 15% of specimen diameter which was 9 mm. Some standard for direct shear test such as ASTM, AASHTO, BS, etc. specify the gap between upper and lower shear box to minimize friction between them. Gap spacing was 1.0 mm in the tests following ASTM standard (ASTM D3080-04, 2011). Curves of shear stress versus horizontal displacement for the direct shear tests are shown in Figure 3.1.

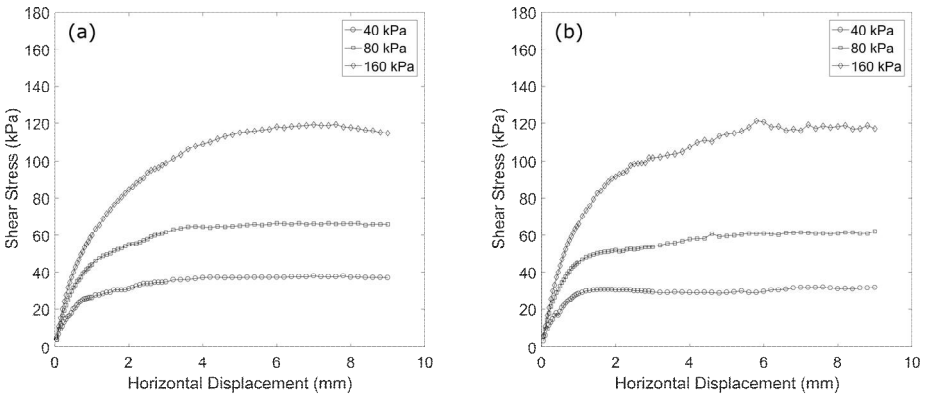

Figure 3.1 Shear stress responses with respect to horizontal displacement from the direct shear tests for (a) the unsaturated soil with 84% relative compaction, (b) the saturated soil with 84% relative compaction

For the tests no peak was appeared. The point where horizontal displacement was 8 mm was considered as failure point of specimen because shear stress remained constant despite the increase in horizontal displacement near this point. The failure envelopes for each cases are shown in Figure 3.2 and strength parameters obtained from the envelope are listed in Table 3.1. From the table, it is apparent that cohesion is significantly decreased as soil saturated, but there is little difference between friction angle of saturated and unsaturated soil. The test results show similar tendency with the study conducted by Kim and Kim (2010). For the unsaturated soil, it is assumed that surface tension between pore water and soil increases apparent cohesion of soil, but it has little effect on friction angle.

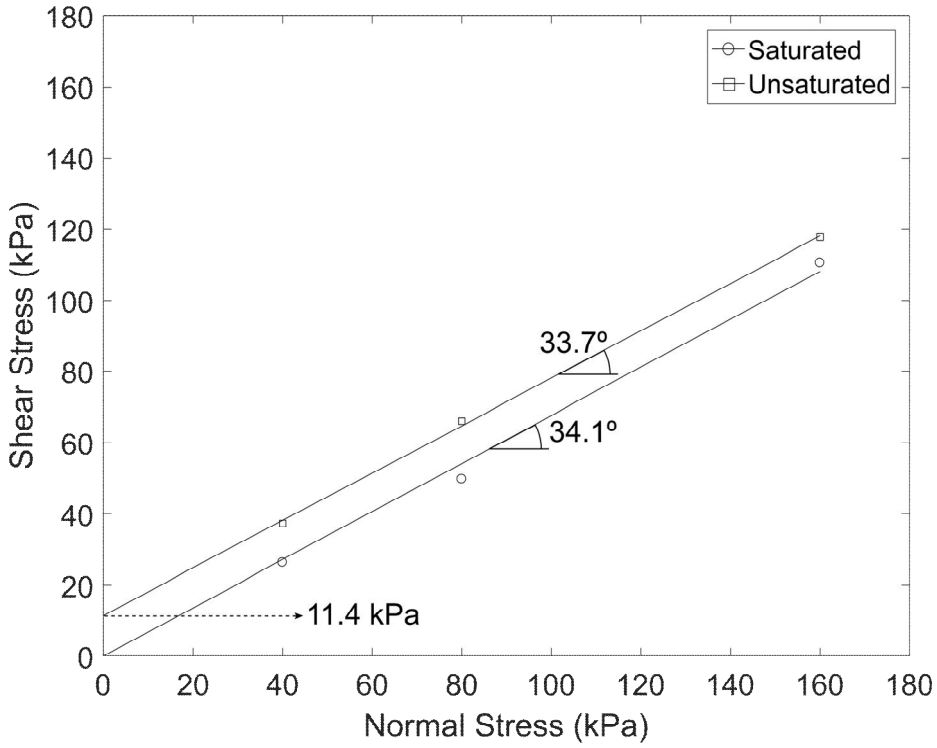

Figure 3.2 Failure envelopes from the direct shear tests for the saturated and unsaturated specimens with 84% relative compaction

Table 3.1 Strength parameters obtained from the direct shear tests

Saturation	ϕ (°)	c (kPa)
Unsaturated	33.7	11.4
Saturated	34.1	0

3.2 Model Test

3.2.1 Test Material

Sewer construction specification specify criteria for backfill material. The criteria are listed in Table 3.2. In the model test, model ground was constructed using soil satisfying the criteria to investigate the influence of saturation and behavior of model ground was investigated.

Table 3.2 Criteria for backfill material

Criteria	Value
Maximum grain size (mm)	100
4.75 mm passing (%)	25 ~ 100
0.075 mm passing (%)	0 ~ 15
Plastic index	0 ~ 10
Degree of compaction	More than 90% relative compaction

Gwanak weathered residual soil was used in the model test. To prevent large-sized particle from distorting behavior of model ground, particles larger than #4 sieve were filtered. As Gwanak weathered residual soil contains 30 to 40% of fine particle, it needed to eliminate fine particle to make the soil meet the criteria for backfill material. Though wet sieving, content of fine particles was lower to 7.5 %. Properties of the soil used in this study are summarized in Table 3.3.

Table 3.3 Properties of the soil used in this study

Criteria	Value
Maximum grain size (mm)	4.75
4.75 mm passing (%)	100
0.075 mm passing (%)	7.5
Max. unit weight of soil (t/m^3)	1.88
Min. unit weight of soil (t/m^3)	1.34
Specific gravity	2.62
USCS classification	SW

3.2.2 Test Method

Schematic diagram of the model test equipment is shown in Table 3.3. The test equipment is consisted of three parts; soil tank, upper water tank and lower water tank. The size of soil tank is 300-mm-wide, 300-mm-long, and 600-mm-high. At the bottom of the soil tank, there is an opening with diameter of 3 mm which simulates crack on a sewer pipe. Through the crack, soil tank and water tanks are connected. When supplying water to upper water tank, lower water tank and pipes connecting water tank and soil tank were filled with water. After that, water was supplied to the soil tank. When supplying water into soil chamber, water head difference between soil tank and upper water tank

was kept 5 cm until it reached to the ground surface to minimize disturbance by water seepage. Considering only the effect of decrease in shear strength of soil following saturation, water drainage was not allowed after water level reached at the ground surface. Instead, water level kept constant while making soil in the soil tank fallen through the crack and stacked at bottom of the lower water tank. In this test, model ground was constructed with 84% relative compaction with the same soil used in the direct shear tests. During the tests, soil loss and shape of the model ground were investigated. After soil loss stopped, final shape of the model ground and amount of soil loss was checked.

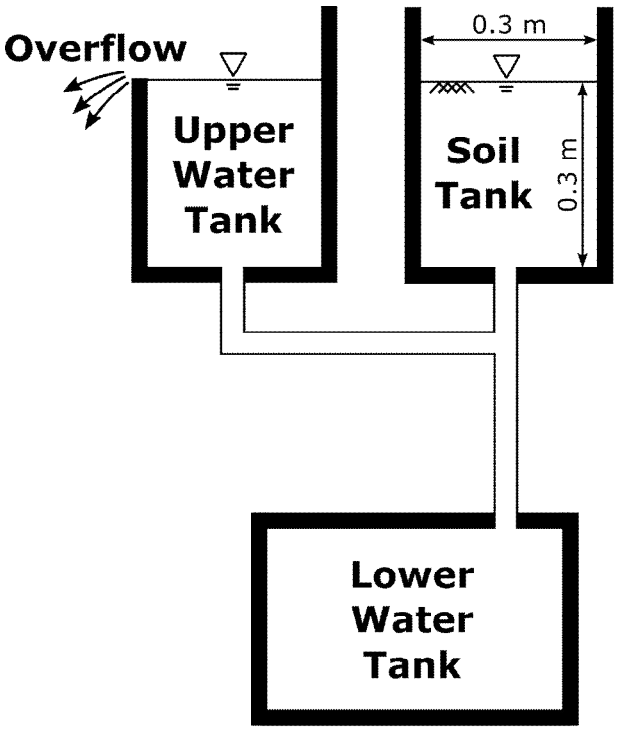

Figure 3.3 Schematic diagram of the model test in this study

3.2.3 Test Result

Until water level reached at the ground surface, soil loss did not occur. After another 20 minutes, soil loss started but ground settlement did not occur at the initial stage. 5 minutes after soil loss started, ground cave-in occurred, and Figure 3.4 showed expansion of ground settlement.

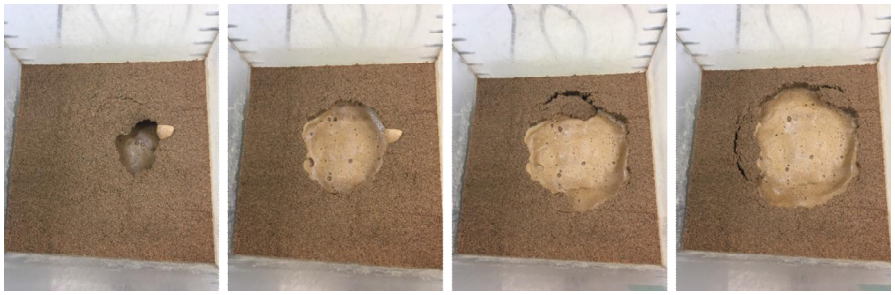

Figure 3.4 Progressive expansion of the ground cave-in in the model test

The expansion of ground cave-in shown in Figure 3.4 occurred within a minutes. Once ground cave-in occurred, ground rapidly collapsed. The model test was concluded when soil loss stopped because of the pipe connecting soil tank and lower water tank blocked by soil. At the end of the test, soil stacked in the lower water tank weighed and almost half the amount of soil was fell apart from the initial ground. Figure 3.5 showed final shape of the ground cave-in of the model test. As shown in Figure 3.5 (a), not only soil in the middle but also soil located in the boundary of the soil tank discharged through the crack and height measured in the middle of the ground was 150 mm. From Figure 3.5 (b), slopes were formed toward the crack located in the middle of the soil tank and pipe was blocked by soil.

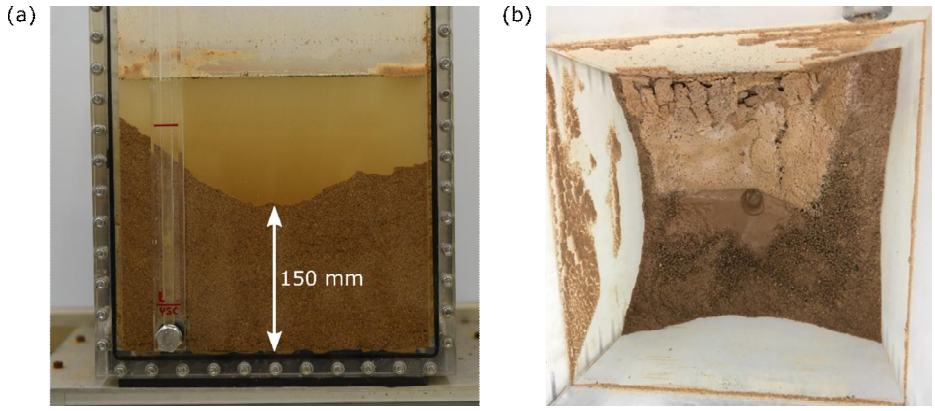

Figure 3.5 Final shape of the ground cave-in of the model test : (a) side-view and (b) aerial view

3.3 Numerical Analysis Using Generalized Interpolation Material Point Method (GIMP)

Problems involving large deformation such as a ground cave-in are not properly solved using the finite element method (FEM) as a result of mesh related problems. In this study Generalized interpolation material point method (GIMP) is used to simulate ground cave-in. In GIMP, the body is discretized into material points, and space is discretized using a background grid. Computation of physical properties is performed using these material points and background grid. Numerical analysis was performed to simulate results of model test and shear strength parameters obtained from direct shear tests were used as input parameters to investigate effects of saturation of soil on the deformation characteristics of soil ground.

3.3.1. Conditions for Numerical Analysis

Figure 3.6 shows initial condition of the analytical model. In this study, axisymmetric model was used to improve efficiency of analysis. The size of model is 300-mm-wide and 300-mm-high. At the bottom of the model, there is an opening with diameter of 3.0 mm which is the same opening size as the soil tank's. Background grid was consisted of squares with 3.0 mm on a side and material point was set as a square with 1.5 mm on as side. In the initial stage of analysis, there were four material points

in one grid. Therefore, in the condition of axisymmetric model, the opening was consisted of five grids, and twenty material points. The movement of side and bottom of the model was laterally and vertically fixed respectively while top was not fixed in any direction. In this analysis only gravitational force was applied to the model. Therefore, gravity caused material points which simulate soil particles to discharge through the opening.

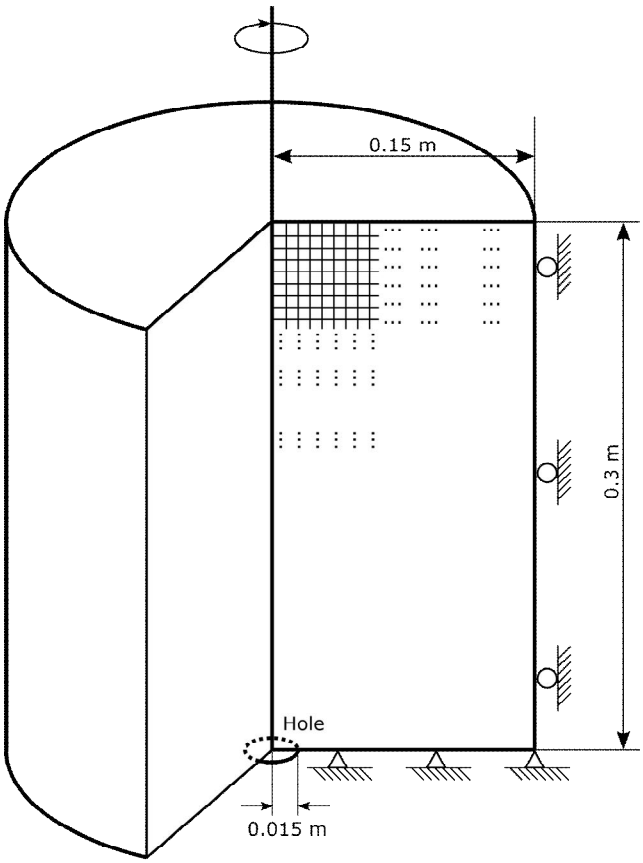

Figure 3.6 Geometry setting of the numerical simulations

To consider only the effect of saturation, seepage force did not be considered in this analysis and assumed the model was fully saturated initially. Mohr-Coulomb plasticity model was used as stress-strain relationship of soil to apply linear failure envelope shown in Figure 3.2. Young's modulus and Poisson's ratio were 500 kPa and 0.2 respectively. In the analysis, friction angle and dilation angle were assumed 34.0° and 3.4° for both saturated and unsaturated soil. Cohesion set as 0.01 kPa for saturated soil and 11.5 kPa for unsaturated soil.

3.3.2 Results of Numerical Analysis

Figure 3.7 shows vertical displacement of the GIMP simulation for unsaturated soil. 0.5 sec after the start of simulation (Figure 3.7(a)), vertical displacement is concentrated near the opening but the amount is slight. There is little additional vertical displacement until 5 sec (Figure 3.7(b)). No soil loss and surface settlement are observed in this simulation.

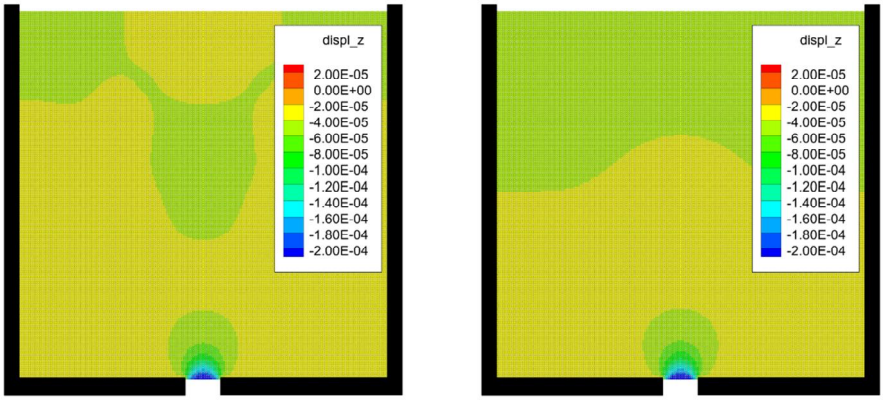

Figure 3.7 Vertical displacement of the GIMP simulation for unsaturated soil specimen at (a) t = 0.5 sec and (b) t = 5 sec

Figure 3.8 to Figure 3.11 show the result of the GIMP simulation for saturated soil specimen. Figure 3.8 shows changes of shape of ground cave-in over time. Unlike unsaturated soil, ground cave-in develops quickly for saturated soil. At the initial stage of simulation, soil loss occurs near the opening (Figure 3.8(a)). As soil keeps discharged from the model, an empty space is expanded vertically which induces surface settlement (Figure 3.8(b), Figure 3.8(c), Figure 3.8(d)). Near the opening, movement of soil particles is disrupted because of interaction between soil particles which causes soil particles to tangle. On the contrary, soil near the surface is discharged without interruption of other soil particles. The difference between rate of soil discharge near the opening and rate of soil discharge near the surface creates two different shear plane (Figure 3.8(e)), a steep slope at the opening and a gentle slope near the top. The difference between two slope angle decreases as soil particle as soil

particles are discharged (Figure 3.8(f), (g), (h)). Two slope converge when soil discharge stops (Figure 3.8(i). Ground cave-in accompanies large deformation shown in Figure 3.8, it is difficult to simulate ground cave-in using finite element method. In that sense, Figure 3.8 shows applicability of GIMP on problems involving large deformation.

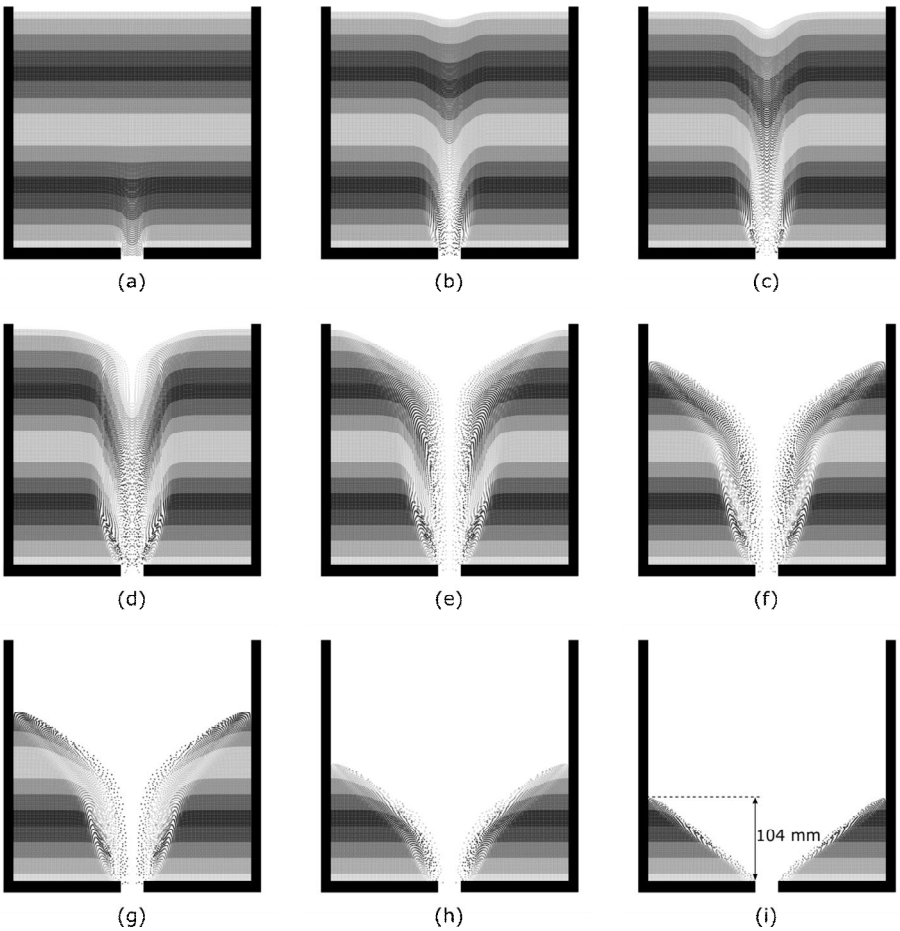

Figure 3.8 Evolution of the ground cave-in in the GIMP simulation for the saturated soil at (a) t = 0.1 sec, (b) t = 1 sec, (c) t = 2 sec, (d) t = 5 sec, (e) t = 10 sec, (f) t = 15 sec, (g) t = 20 sec, (h) t = 30 sec, and (i) t = 50 sec

Figure 3.9 and Figure 3.10 show radial and vertical displacement in the GIMP simulation respectively. At the beginning of simulation, displacements occur near the opening (Figure 3.9(a), Figure 3.10(a)). As soil particle discharged, radial displacement occurs at the ground surface and expands quickly (Figure 3.9(b), (c), (d)). Vertical displacement spreads quickly toward ground surface after 1 sec (Figure 3.10(b), (c), (d)). There is a space where radial displacement does not occur while vertical displacement occurs slightly at Figure 3.9(c) and Figure 3.10(c). This area signifies that soil particles move downward as a soil block without internal displacement of the block. After ground surface settlement occurs, radial displacement near the surface is more widely distributed than vertical displacement (Figure 3.9(d), Figure 3.10(d)). There is less inter-particle disruption near the surface than near the opening which makes the difference of particle discharge rate and causes radial displacement larger than vertical displacement.

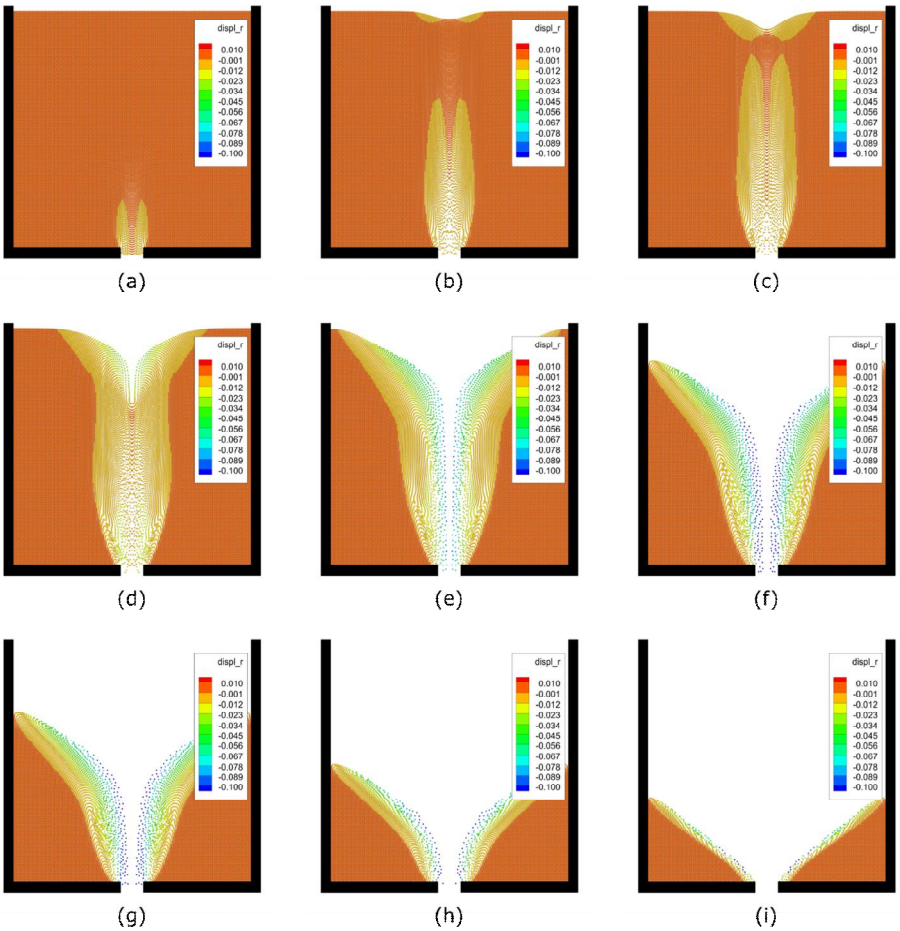

Figure 3.9 Radial displacement in the GIMP simulation for the saturated soil at (a) t = 0.1 sec, (b) t = 1 sec, (c) t = 2 sec, (d) t = 5 sec, (e) t = 10 sec, (f) t = 15 sec, (g) t = 20 sec, (h) t = 30 sec, and (i) t = 50 sec

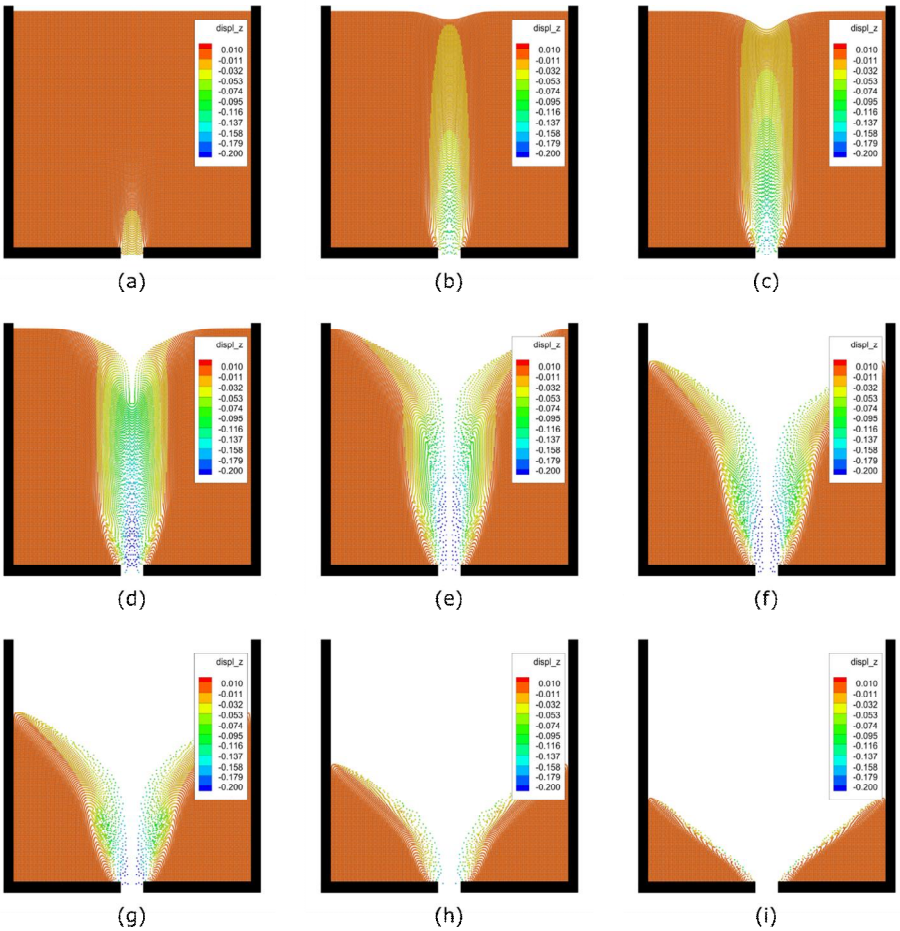

Figure 3.10 Vertical displacement in the GIMP simulation for the saturated soil at (a) t = 0.1 sec, (b) t = 1 sec, (c) t = 2 sec, (d) t = 5 sec, (e) t = 10 sec, (f) t = 15 sec, (g) t = 20 sec, (h) t = 30 sec, and (i) t = 50 sec

Figure 3.11 shows equivalent plastic shear strain in GIMP simulation. Equivalent plastic shear strain is concentrated near the opening at initial stage (Figure 3.11(a)). The distribution quickly spreads toward the ground surface as soil particles are discharged (Figure 3.11(b), (c)).

There is an area where equivalent plastic shear strain is very small near the ground surface. As discussed before, in this area, soil particles move as a block which leads to small equivalent plastic shear strain (Figure 3.11(c)). As soil leakage continues, two different failure planes are formed. A steep failure plane is formed at the bottom of the model because soil particle interaction disrupts soil leakage near the opening while a gentle failure plane is formed at the top as there is less soil particle interaction (Figure 3.11(e), (f)). The angles of two different failure plane are converge when soil leakage stops (Figure 3.11(i)).

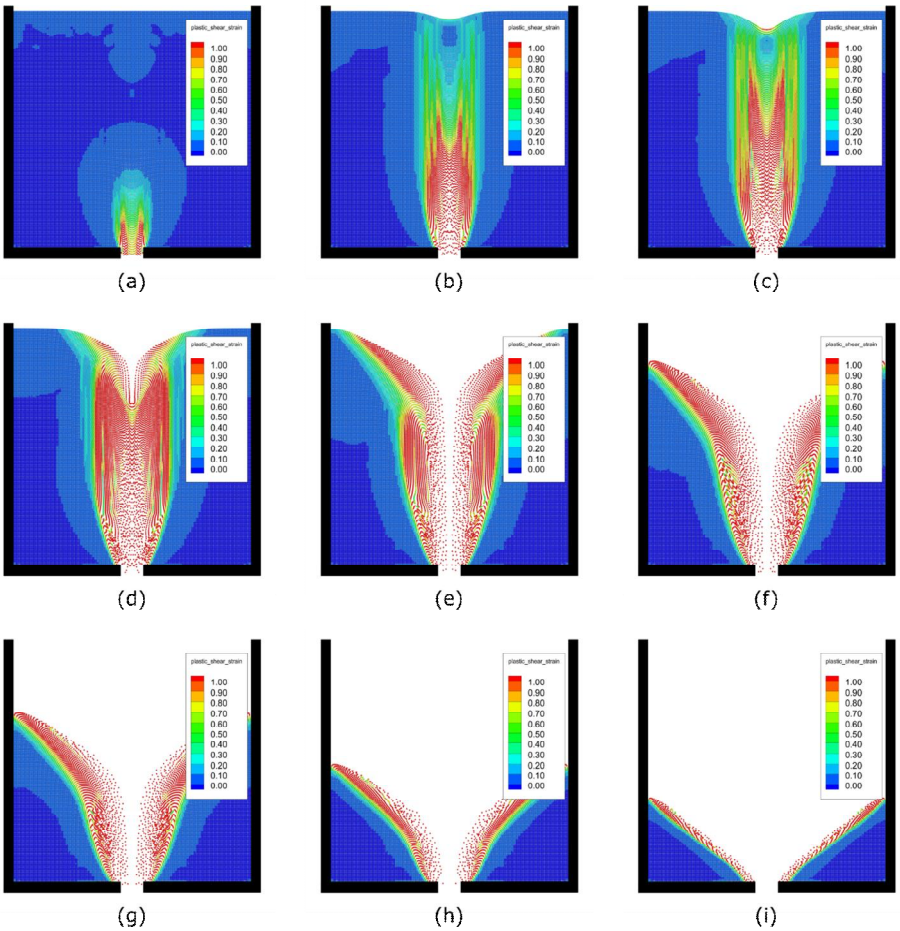

Figure 3.11 Equivalent plastic shear strain in the GIMP simulation for the saturated soil (a) t = 0.1 sec, (b) t = 1 sec, (c) t = 2 sec, (d) t = 5 sec, (e) t = 10 sec, (f) t = 15 sec, (g) t = 20 sec, (h) t = 30 sec, and (i) t = 50 sec

3.4 Discussion

Before water supply to the model ground, ground was in unsaturated condition and no soil discharge occurred. In the case of numerical simulation, there was no soil leakage and ground settlement when unsaturated soil strength parameters were used. It is assumed that tensile force applied to soil is resisted by apparent cohesion created by surface tension of pore water. At the beginning, soil discharge occurred near the opening in both model test and numerical analysis. Empty space was formed as soil leakage continue which caused ground settlement. Soil located on the top of the model discharged rapidly through vertically formed empty space and size of ground cave-in enlarged. In this sense model test and numerical analysis show similarity, however, difference in boundary conditions, exclusion of seepage analysis and incomplete saturation caused some differences of behavior of soil

1) In model test, soil leakage slowly occurred after ground water level reached ground surface. While soil leakage occurred within a minute in numerical analysis. To make soil saturate, ground was immersed in water without vacuum pressure. It is assumed that this procedure cannot guarantee fully saturated soil and ground is gradually saturated during the model test. Therefore, apparent cohesion could be bigger than expected and it could delay soil discharge. Also, soil particle could be rapidly discharged because interaction between soil and water such as buoyancy was not considered in numerical analysis.
2) In numerical analysis, the height of ground at the end of the simulation was 104 mm and the opening was exposed. Also

almost 77% of soil discharged. In the case of model test, the height of ground was 150 mm and the opening was no exposed, it covered by soil. Also, nearly 50% of soil discharged. In the model test, the pipe connecting soil tank an lower water tank was plugged by soil which made the differences.

3) A rectangular soil tank was used in model test, while cylinder shaped soil tank was assumed in numerical analysis to use axisymmetric condition. This is reason why final shape of ground is different.

Chapter 4 Conclusions

This study presents direct shear tests, model tests and numerical simulations to assess the effect of reduction of soil strength by saturation during formation of ground cave-in caused by damaged sewer pipe. Direct shear tests were performed to evaluated strength parameter change in relation to saturation rate. The tests results show that the saturation affects the cohesion of soil significantly while it has little influence on the friction angle of soil. To experimentally simulate the effect of reduction of soil strength by saturation on ground cave-in, model tests were performed. In the model tests, water level slowly rose to the ground to exclude the effect of seepage and maintained to the ground using external water tank acting like a weir. There was no soil leakage until water level reached to the ground. Soil leakage occurred a few minutes after water level maintained, ground settlement occurred and size of ground cave-in enlarged as soil discharged. In this study, application of GIMP on the simulation of ground cave-in was assessed. As ground cave-ins are accompanied with extreme deformation, conventional finite element method has difficulty to simulate them. Though there are differences between the model test and numerical simulation caused by boundary conditions, incomplete saturation, and exclusion of seepage analysis, similar ground deformation characteristics are observed in the model test and numerical simulation. Ground cave-ins are occurred not only by reduction of soil strength by saturation but also by seepage force applied by groundwater flow. Therefore, to achieve more

reliable numerical simulation results, the effect of groundwater flow should be considered and multiple physical GIMP analysis should be performed.

Reference

1. ASTM D3080-04. (2011). “Standard Test Method for Direct Shear Test of Soils Under Consolidation Drained.” Annual Book of ASTM Standards, 1-7.
2. Bardenhagen, S. G., and Kober, E. M. (2004). “The Generalized Interpolation Material Point Method.” Computer Modeling in Engineering & Sciences, 5(6), 477–495.
3. Fredlund, D. G., Rahardjo, H. & Fredlund, M. D. Unsaturated Soil Mechanics in Engineering Practice (Wiley, 2012)
4. Kim, M., and Kim, Y. (2010). “Shear Strength of Weathered Granite Soil Considering Change of Saturation.” Journal of the Korean Geoenvironmental Society, 11(9), 5–14.
5. Kuwano, R., Sato, M., and Sera, R. (2010). “Study on the Detection of Underground Cavity and Ground Loosening for the Prevention of Ground Cave-in Accident.” Japanese Geotechnical Journal, 5(2), 349–361.
6. Rogers, C. (1986). Sewer deterioration studies the background to thestructural assessment procedure in the sewerage rehabilitationmanual. WRC Report ER199E.
7. Seoul Metropolitan Goverment. (2017). “Seoul metropolitan goverment invests 130.6 billion won to repair sewage pipe lines to prevent ground cave-ins.” Seoul Metropolitan Goverment Press Releases, Seoul.

초록

최근 도심지에서 지반함몰에 의한 인적, 물적 피해가 증가함에 따라 지반함몰은 도심지 지반재해로서 주목을 받고 있다. 도심지에서 발생하는 지반함몰은 하수관 손상으로 인해 발생하는 경우가 대다수이다. 노후화 등에 의해 파손이 발생한 관 내부가 강우 등으로 가득차면 하수가 손상부를 통해 지반으로 유출되고, 이로 인해 지하수위가 상승하여 지반의 포화도가 증가하게 된다. 초기 불포화 상태에 있던 지반이 포화되면 모관흡수력의 상실로 인해 흙의 강도가 저하하여 토사 유실이 발생하게 되고, 이로 인해 지중 공동 및 지반함몰이 발생하게 된다. 본 연구에서는 지반의 포화도 상승으로 인한 흙의 강도 저하가 지반함몰 발생에 미치는 영향을 확인하기 위하여 모형실험과 수치해석을 수행하였다. 모형실험의 경우 기존에 국내외에서 수행되었던 실험과 달리 물의 하향 침투에 의한 침투압의 영향을 배제하고자 지반 내로 물을 유입시키는 과정만 수행하고 유출시키는 과정은 생략하였다. 지반함몰과 같은 대변형을 유발하는 문제를 유한요소법으로 해석할 경우, 격자의 왜곡 및 뒤틀림 등으로 수치적분의 정확도가 감소할 수 있고 누적된 오류로 해석이 중단될 수 있다. 따라서 유한요소법의 대안으로 대상체를 요소가 아닌 유한개의 재료점으로 분해하고, 공간은 배경격자로 이산화 하는 Generalized Interpolation Material Point Method (GIMP)를 이용하여 지반함몰을

모사하였다. 비록 경계조건의 차이, 불완전한 포화, 손상부 연결관의 폐색 등에 의해 함몰 시간 등에는 차이가 있었지만, 토조모형시험과 수치해석에서 유사한 변형 거동을 확인할 수 있었다.

주요어 : 지반함몰, 흙의 강도, 포화도, GIMP, 모형시험

학번 : 2015-22929